Contents

1 Bioenergetic model

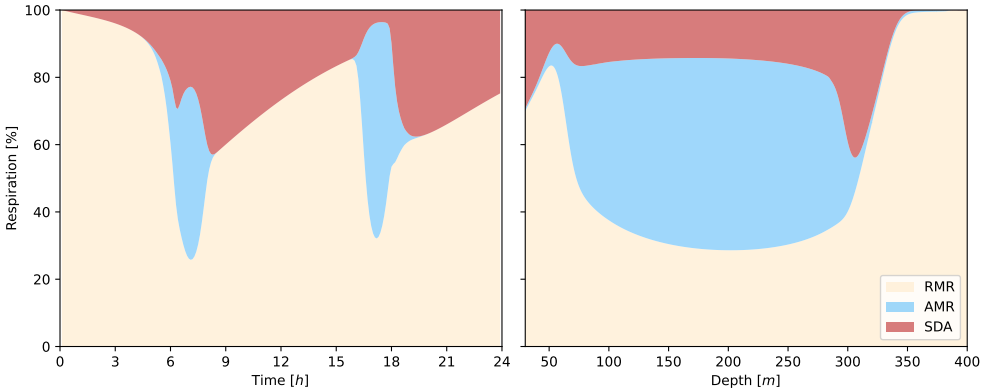

Figure S1: Relative importance of the respiration rates depending on micronekton activity: resting (RMR), swimming (AMR) and feeding (SDA). The parameters of this simulation correspond to a fish of 35mm.

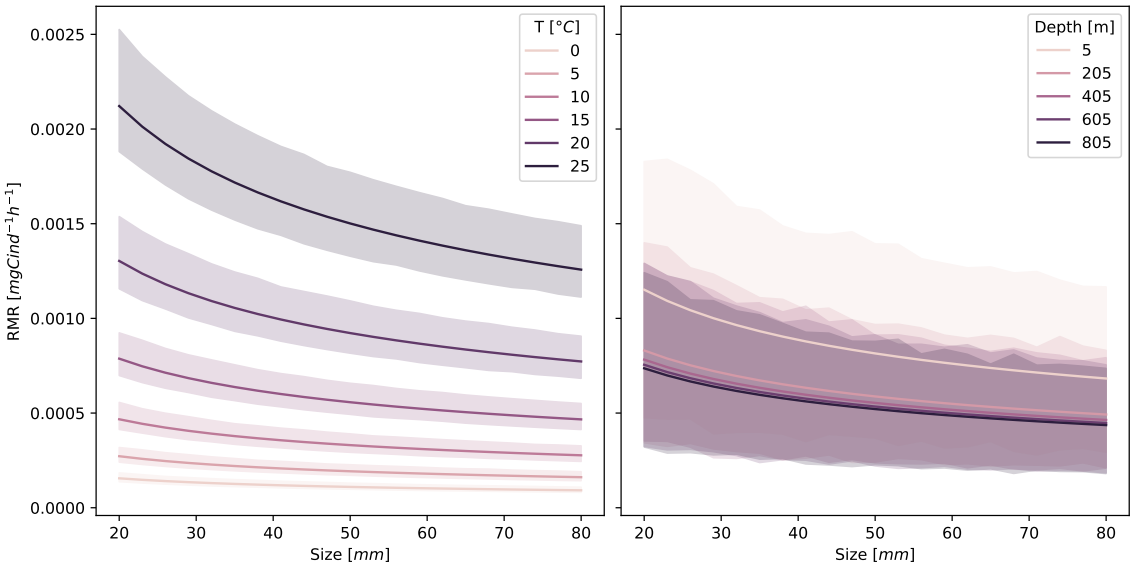

Figure S2: Routine respiration rates (RMR) as a function of size, temperature and depth. Here as an example for a fish from Eq.5.

Detritus pools (%)	Fish	Crustacean	Cephalopod
Respiration	50.0±8.8	39.2±8.5	60.5±9.5
Fecal pellets	21.0±1.3	26.0±2.4	9.6±0.3
Dead bodies	28.9±7.7	34.8±10.7	29.9±9.75

Table S1: Summary statistics of the relative contribution of the carbon detritus produced by micronekton of different sizes. Mean values are represented with their standard deviation. These values correspond to those represented in Fig.4.

Table S2: Respiration coefficients used to calculate respiration rates for the different taxonomic groups: Fish (F), Crustacean (A) and Cephalopod (S). Mean values correspond to those used in the simulations as indicated in Table.2 and the standard error (std) was added to or subtracted from the mean to define the range of these parameters for the sensitivity analysis.

Symbol	Mean (std)	Group	Source
a_0	30.767 (2.451)	F	Ikeda (2016)
a_1	0.870 (0.020)	F	Ikeda (2016)
a_2	-8.515 (0.737)	F	Ikeda (2016)
a_3	-0.088 (0.031)	F	Ikeda (2016)
a_0	24.461 (5.820)	S	Ikeda (2016)
a_1	0.868 (0.054)	S	Ikeda (2016)
a_2	-6.424 (1.650)	S	Ikeda (2016)
a_3	-0.261 (0.064)	S	Ikeda (2016)
a_0	23.079 (0.970)	A	Ikeda (2014)
a_1	0.813 (0.013)	A	Ikeda (2014)
a_2	-6.248 (0.280)	A	Ikeda (2014)
a_3	-0.136 (0.011)	A	Ikeda (2014)

2 Modeling irradiance

Surface irradiance (I_0 in Eq.2,4) was modelled as a periodic function of time t, varying over the day as follows,

$$I_0(t) = 1 - \exp(-asin(\omega t)^n) \tag{1}$$

with $\omega = (2\pi)/2H$ where H=24h, the parameter n=25, defining the timing of twilight hours, and the parameter $a = 200$, defining the degree of flattening of the curve. The sinusoid has a flattened shape, allowing a null migration speed during the day and night (Fig.S3, 2).

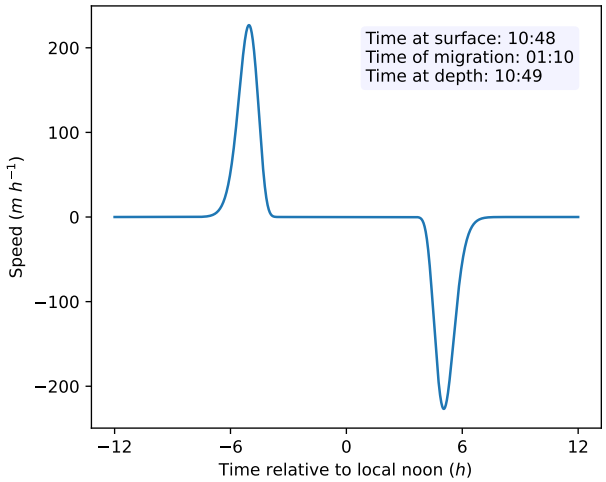

Figure S3: Relative daily migration speed for a fish measuring 35mm. A positive swimming speed causes organisms to go down to the bottom of the water column, and a negative speed causes them to rise to the surface. Time spent at the surface, at depth and migrating are calculated.

The parameter n varies annually according to the time of sunrise and sunset, calibrated with the winter solstice in December, when days last 6 hours, and during the summer solstice in June, when daylight last 12 hours at PAP-SO,

$$n = (n_{max} - n_{min})\frac{cos(\omega(t+T)+1)}{2} + n_{min} \tag{2}$$

with $\omega = (2\pi)/T$ where T=365 j, $n_{max} = 60$ and $n_{min} = 14$.

The annual surface irradiance was finally computed with the annual variation of the solar angle following the cosine law,

$$I_{year}(t, 0) = I_0(t)cos(\phi) \tag{3}$$

where ϕ is the solar angle as a function of latitude, longitude and time of the year.

Annual irradiance along depth z was computed for the visual predation rate based in Eq.5,

$$I_{year}(t, z) = I_{year}(t, 0)e^{-K_{d490}(z).z} \tag{4}$$

The attenuation coefficient was defined from the empirical equation of Morel et al. (2007),

$$K_{d490}(z) = 0.0166 + 0.072\ Chl(z)^{0.69} \tag{5}$$

where Chl is the chlorophyll a concentration along the water column in mg m^{-3} at PAP-SO, from Copernicus Marine Service Information (CMEMS).

3 Relative effects of seasonal parameters

The relative influence of the three environmental factors on carbon production was investigated separately. This results in three simulations showed in Fig.S4, each varying one of the environmental factors over the year, the other two remaining stable over the seasons (Table.S3).

Scenarii	**Seasonal variation**			
	PP	**Temp.**	**Light**	c_α
Scenario 1	X			3
Scenario 2		X		3
Scenario 3			X	0.002
Scenario 4	X	X	X	0.045

Table S3: Seasonal simulations involving both independent and dependent variation of the environment conditions with the scaling coefficient c_α, used to calculate the visual capture rate in Eq.5.

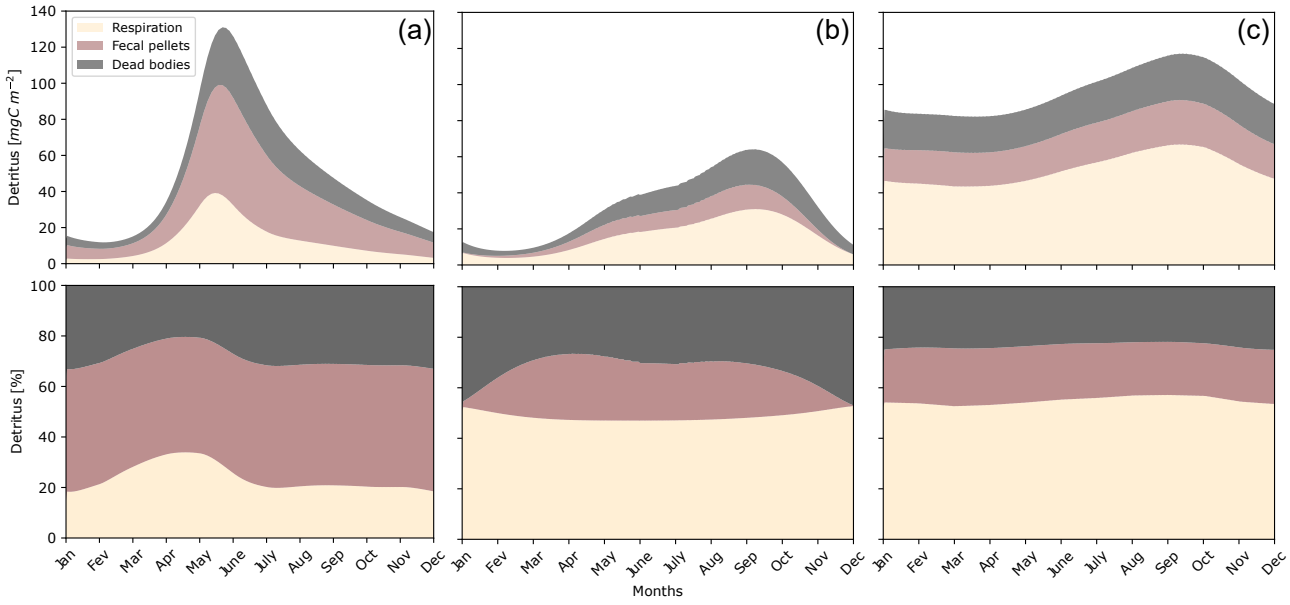

Figure S4: Annual carbon production of seasonal variations simulated independently for each environmental variable: phytoplankton concentration (a), light (b) and temperature (c). Carbon production is integrated along depth, including respiration (D_m), fecal pellets (D_g) and dead bodies (D_μ).

Seasonal variation of phytoplankton concentrations generated a strong peak of detritus production in May that reached 130 mgC m^{-2} (Fig.S4a). This peak then attenuated until it reached its lowest values in January, of 18 mgC m^{-2}. The proportion of the metabolic products was almost twice higher during spring compare to the rest of the year, from 20% to 40%. On the opposite, the proportion of dead bodies production reduced during this period, from 30% to less than 20%. The proportion of fecal pellets production remained stable over the year, around 52% of the total carbon production induced by micronekton.

Variation of temperature had a less pronounced effect than the phytoplankton concentration on detritus production with a maximum of 120 mgC m^{-2} in September and a minimum of 85 mgC m^{-2} in January (Fig.S4b). The proportions of the three different carbon detritus were stable during the year with a slight increase in the percentage of respiration in summer. Respiration as DIC represented almost 55% of the total carbon production, fecal pellets 25% and dead bodies 20%.

Independent variation of light generated a peak of carbon production in late summer of 70 mgC m^{-2} corresponding to maximum light intensity and shortest nights (Fig.S4c). The proportion of fecal pellets is lower compared to the other scenarios and tends to zero in December-January. The proportion of respiration is around 50% over the year, similar to the second scenario.

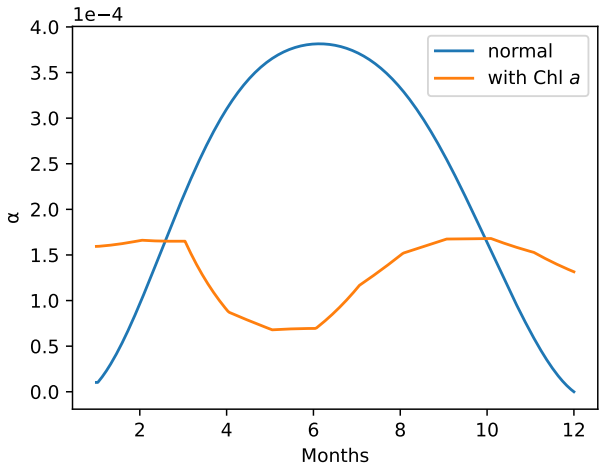

Figure S5: Variation of the capture rate α at 40 m over a year based on two environmental conditions. The blue curve corresponds to the computation of the capture rate from Eq.S4 and Eq.S5 with a constant attenuation coefficient, used for Fig.S4c. The orange curve corresponds to the computation of the capture rate with the attenuation coefficient, function of Chl *a* concentrations (Eq.S5) used for Fig.7 and Fig.8.

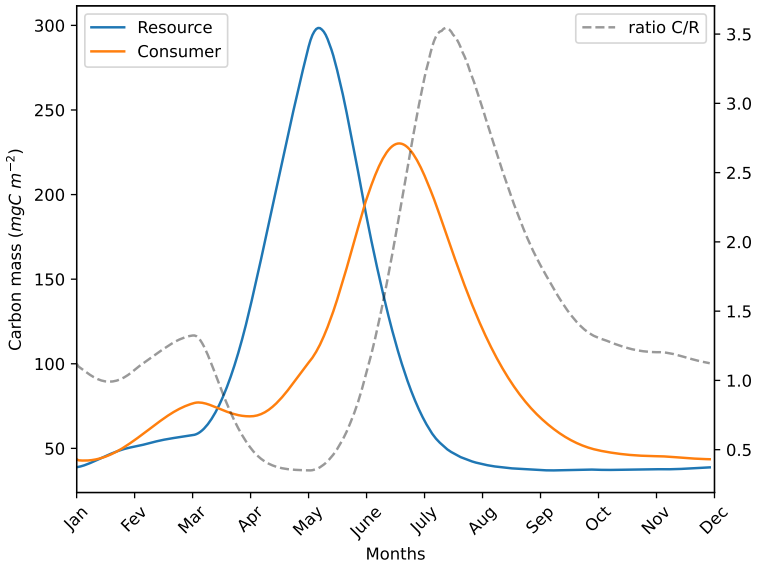

Figure S6: Carbon concentration of the resource (R) and the consumer (C) with environmental variations over the year. This corresponds to the simulation of the carbon production observed in Fig.7,8.

4 Size and biomass distribution

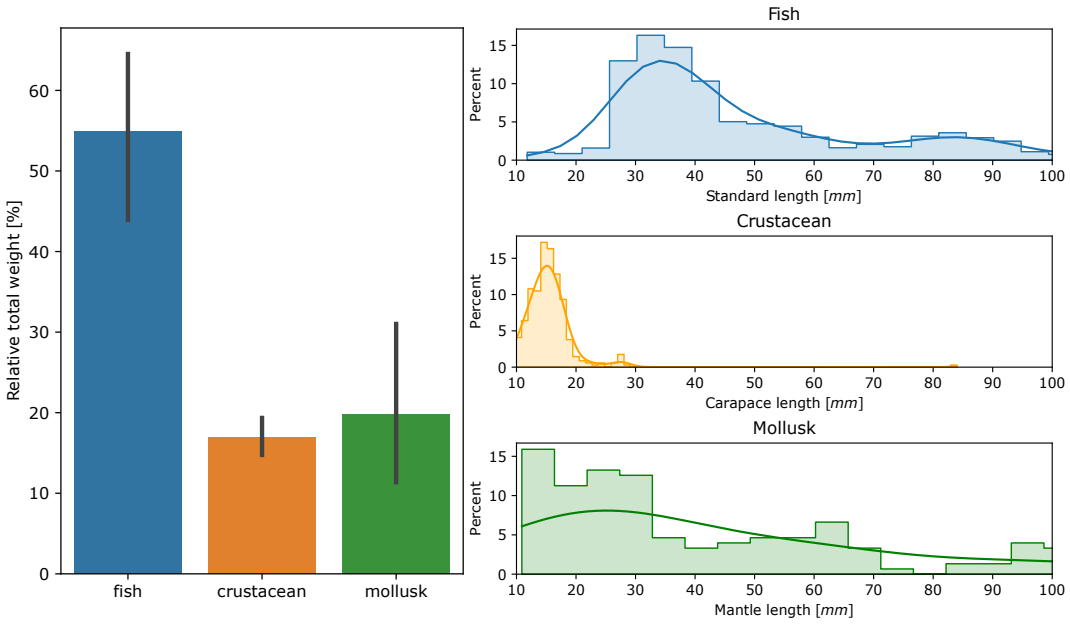

Figure S7: Weight and size distribution of three micronekton taxonomic groups (fish, crustacean and mollusk) collected with a mid-water trawl during the APERO cruise (com. pers.). The variability of the relative total weight comes from the differences between the stations.

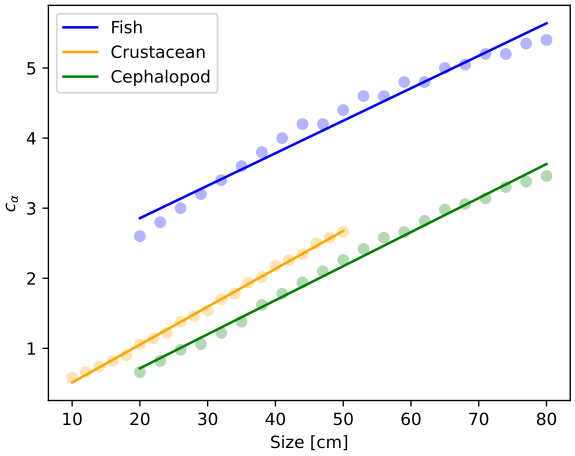

Figure S8: Capture rate coefficient (c_α) depending on the size for each micronekton taxonomic groups (fish, crustacean and cephalopod). The visual capture rate depends on the relative gradient of light and a scaling coefficient (c_α). This coefficient was calibrated for each simulations with variation of size and taxonomic group in Fig.3.

References

Ikeda, T.: Respiration and ammonia excretion by marine metazooplankton taxa: synthesis toward a global-bathymetric model, Marine biology, 161, 2753–2766, https://doi.org/10.1007/s00227-014-2540-5, 2014.

Ikeda, T.: Routine metabolic rates of pelagic marine fishes and cephalopods as a function of body mass, habitat temperature and habitat depth, Journal of Experimental Marine Biology and Ecology, 480, 74–86, https://doi.org/10.1016/j.jembe.2016.03.012, 2016.

Morel, A., Huot, Y., Gentili, B., Werdell, P. J., Hooker, S. B., and Franz, B. A.: Examining the consistency of products derived from various ocean color sensors in open ocean (Case 1) waters in the perspective of a multi-sensor approach, Remote Sensing of Environment, 111, 69–88, https://doi.org/10.1016/j.rse.2007.03.012, 2007.